Structural phase transitions in aluminium above 320 GPa

Guillaume Fiquet, Chandrabhas Narayana, Christophe Bellin, Abhay Shukla, Imène Esteve, Art Ruoff, Gaston Garbarino, Mohamed Mezouar

Structural phase transitions in aluminium above 320 GPa

G. Fiquet [1]*, C. Narayana[2], C. Bellin[1], A. Shukla[1], I. Estève[1], A.L. Ruoff[3], G. Garbarino[4] and M. Mezouar[4]

[1] *IMPMC, Sorbonne Université, UMR CNRS 7590, Muséum National d'Histoire Naturelle, IRD, 4 Place Jussieu, 75252 Paris cedex 05, France.*

[2] *Chemistry and Physics of Materials Unit, Jawaharlal Nehru Centre for Advanced Scientific Research, Jakkur P.O., Bangalore 560064, India.*

[3] *Materials Science and Engineering, Cornell University, Ithaca, NY 14853-1501, USA.*

[4] *European Synchrotron Radiation Facility, BP 220, F-38043 Grenoble Cedex, France.*

Provide full correspondence details here including e-mail for the *corresponding author:

*corresponding author: Guillaume Fiquet, IMPMC UMR CNRS 7590, Sorbonne Université, CNRS, Campus Pierre et Marie Curie, 4 Place Jussieu, 75005 Paris, France.

Email: guillaume.fiquet@sorbonne-universite.fr

Structural phase transitions in aluminium above 320 GPa

With the application of pressure, a material decreases in volume as described in its equation of state, which is governed by energy considerations. At extreme pressures, common materials are thus expected to transform into new dense phases with extremely compact atomic arrangements that may also have unusual physical properties. For aluminium, first principle calculations have consistently predicted a phase transition sequence fcc - hcp - bcc in a pressure range below 0.5 TPa (1-7). The hcp phase was identified at 217 GPa in an experiment (13) and the bcc phase has been recently confirmed in a dynamic ramp-compression experiment coupled with time-resolved X-ray diffraction (16). Here we confirm this observation with a synchrotron-based X-ray diffraction experiment carried out within a diamond-anvil cell and report indications of the onset of the transition towards a bcc structure at pressures beyond 320 GPa. With this work, we also demonstrate the possibility of routine static high-pressure experiments with conventional bevelled diamond-anvil geometry in the 0.3-0.4 TPa regime.

Keywords: aluminium, structural transition, x-ray diffraction, multi-megabar

Introduction

The extreme pressure phase diagram of materials is important not only for the understanding of the interiors of planets or stars, but also for the fundamental understanding of the relation between the crystal and electronic structures. Structural transitions induced by extreme pressures are governed by the deformation of the charge

density of the valence electrons which bears the brunt of the increasing compression while the relative volume occupied by the nearly incompressible ionic core electrons increases. This fact is said to hold not only in the few hundred GPa range but also beyond the terapascal regime where compression pushes ion cores together. Experimental limitations will however keep the TPa regime in the realm of predictions, at least as far as static pressure is concerned.

Early first principles calculations (1) for aluminium (Al) predicted an *fcc* -> *hcp* -> *bcc* structural transition trend over a pressure range of roughly 0–500 GPa and these have since been repeatedly confirmed (2-4) and refined (5-7). This non-intuitive generic transition from a compact (*fcc* or *hcp*) to a more open (*bcc*) structure with increasing pressure is said to be driven by the increasingly smaller and restricted volume available for the valence electrons. This tends to reduce electronic bandwidth by the occupation of an *s*-*d* band at a few hundred GPa (as opposed to the dispersive *s*-*p* band at low pressures). Ultimately, theoretical calculations indicate that valence electrons can be localized in "interstitial" spaces in an open-packed incommensurate host-guest structure similar to that predicted at 3.2 TPa (8). That *d* electrons play a role in these transitions is strongly suggested by the fact that the structure sequence with increasing pressure is mirrored in transition metals as the number of d electrons increases (9) (the analogy has obvious limitations since the underlying magnetism intervenes in transition metals (10)). As the unit cell volume is reduced to fractions approaching half or less, the initially unoccupied *d* bands in simple metals and in particular in aluminium approach, narrow, and descend below the Fermi level triggering structural changes which can be intuitively understood since the *bcc* structure is more compatible with a bonding interaction between second nearest neighbour atoms than the *fcc* structure (1,2). Such a transition has earlier been reported in Mg (11) and Pb (12) where it takes place at lower

pressures.

A simple system like Al is not only important as a benchmark for theory, but can also be used as a standard for pressures in the TPa range and beyond, which are targeted at dynamic compression facilities such as the National Ignition Facility (NIF) at the Lawrence Livermore National Laboratory in the US or Laser Mégajoule (LMJ) in Bordeaux in France. Confirming predictions of aluminium structure at extremely high densities is thus paramount. According to a recent first principle calculation (7), aluminium should undergo a phase transition from *fcc* to *hcp* structure around 200 GPa and another transition from *hcp* to *bcc* with further compression beyond 300 GPa. The hcp phase around 217 GPa was reported in an earlier room-temperature static high-pressure experiment where a maximum pressure of 330 GPa was achieved (13). An earlier classical shock-compression study found no evidence of the predicted *fcc* to *hcp* transition (14) but it is expected that *fcc* aluminium melts at 125-150 GPa along principal Hugoniot (see (16)). More recently, *bcc* aluminium has been synthesized in the non-equilibrium conditions of an ultra-fast laser-induced micro-explosion confined inside a sapphire (α-Al_2O_3) rod (15). This recent report of the *bcc* super-dense phase of Al is interpreted as a complex route of synthesis via a spatial separation of Al and O ions in short-lived hot non-equilibrium plasma of solid-state density. The micro-explosion confined inside a sapphire capsule leads to this *bcc*-Al phase, which survives in a compressed state after fast quenching. However, if confined micro-explosions provide an interesting route to create and recover high-density polymorphs, such an experiment does not allow the determination of a transition pressure nor does it show any evidence of the presence of a quenched *hcp* phase. Very recently, an experiment succeeded to combine nanosecond *in situ* x-ray diffraction and simultaneous velocimetry measurements to determine the crystal structure and pressure of ramp-

compressed aluminium at stress states between 111 and 475 GPa (16). The solid-solid Al phase transformations, fcc–hcp and hcp–bcc, are reported at 216 ± 9 and 321 ± 12 GPa, respectively. In this article, we confirm this observation with a synchrotron-based X-ray diffraction experiment carried out within a diamond-anvil cell and report indications of the onset of the transition towards a bcc structure at pressures beyond 320 GPa.

Experimental

Sample preparation

Central to our experiment was the establishment of a protocol for reaching pressures exceeding 350 GPa in a diamond-anvil cell with a pure aluminium sample (Fig. 1) confined inside a conventional gasket (Fig. 2), which limits the deviatory stress component to moderate values. Very fine-grained aluminium powder is very difficult to handle and is pyrophoric in nature. It can thus easily oxidize. We used instead an aluminium foil (99.999 % purity, 15 µm thick, Goodfellow) as starting material. Samples were pre-cut from this foil with a focused ion beam (FIB) so as to obtain cylinders (Fig. 1) with dimensions fitting the holes prepared in pre-indented rhenium gaskets.

High-pressure cells preparation and sample loading

Our experiments were conducted in symmetrical diamond anvil cells equipped with single bevelled diamonds (8° bevel) mounted on X-ray transparent cubic boron nitride seats. Two separate experimental runs were carried out at ambient temperature with diamonds having centre flat culets of 35 and 20 µm diameters respectively. The first

experiment with the 35 μm culet anvil reached 257 GPa whereas the second one reached pressures of about 370 GPa. In our experiments, no pressure-transmitting medium was used. As noted by Akahama et al. (13), Al has a relatively low shear modulus and is expected to keep low uniaxial stresses in the diamond-anvil cell. Success of experiments in this pressure range are highly dependent on handling samples inside a hole of less than 10 μm, which has to be perfectly centred on a culet of 20 μm made on a gasket pre-indented to less than 10 μm. Manipulating a sample of such small dimensions inside a highly contoured gasket terrain to place it perfectly into the hole is yet another challenge. In the present experiment, we have used the focused ion beam for drilling such tiny holes (see 17) in rhenium with a centring precision better than 1 μm and causing very little defects to the gaskets. Rhenium gaskets were pre-indented to reach an initial thickness of about 12 μm, and then drilled with the focused ion beam (FIB). Preparation of gaskets and sample loading were carried out in the FIB chamber, so as to have a perfect sample loading in the pressure chambers (see Fig. 2). Above 300 GPa, pressure was estimated according to the equation of state of rhenium (18). In the *fcc* stability field, pressure was measured with available equations of state reported for aluminium (13, 19). Both methods yield pressure measurements in very good agreement (*i.e.* within error bars) up to 300 GPa. Alternatively, the equation of state for rhenium proposed by Dubrovinsky et al. (20) could be used but the latter yields significant pressure overestimate when compared to other measurements (as large as 70 GPa at 300 GPa).

X-ray diffraction experiments

In situ X-ray diffraction high-pressure experiments were conducted at the high-pressure beamline ID27 of the European Synchrotron Radiation Facility (ESRF, Grenoble,

France). X-ray diffraction pattern were collected using an angle dispersive monochromatic set-up with a wavelength of 0.3738 Å (iodine K-edge at 33.3 keV) focused with KB mirrors down to a spot of 2.5 x 3 μm FWHM at sample location. Such a spot size explains why rhenium diffraction lines are completely absent in the first run conducted with bevelled diamonds with a central culet of 35 μm in diameter and a sample chamber of 14 μm in diameter which reached a pressure of 240 GPa (see Fig. 3). Rhenium lines are visible in the second run designed to reach a higher pressure (Fig. 5) with a smaller sample having a diameter of about 8 μm mounted on 20 μm culets. Exposure time varied from 60 s below 100 GPa to 240 s at pressures exceeding 370 GPa, thus compensating for the thickness reduction as pressure was increased. We used a two-dimensional MAR CCD detector located at a distance of 207 mm from the sample. Images were then integrated using the Fit2D software (21) in order to obtain a conventional diffraction pattern. Data analysis was then carried out using the GSAS package (22, 23). Cell parameters were refined using LeBail method for the extraction of reflection intensity. Preferred orientations were not refined. Graphics were realized with the Datlab software (courtesy K. Syassen, MPI Stuttgart). All X-ray diffraction patterns are background subtracted.

Results and discussion

X-ray pattern analysis

The first run presented in Fig. 3 show a smooth evolution of the *fcc* structure at lower pressures. The pattern at 213 GPa can be unambiguously assigned to a *fcc* lattice with a lattice parameter a= 3.246 (1) Å and a unit cell volume of 34.190 (31) $Å^3$. With four atoms per unit cell in the *fcc* structure, the atomic volume is 8.548 $Å^3$. As pressure was

165 increased, new peaks appeared around 220 ± 5 GPa. At the pressure of 235 GPa, as
166 shown in Fig. 4, these new lines can be unambiguously assigned to a *hcp* structure with
167 lattice parameters a= 2.266 (1) Å and c=3.720 (2) Å and a unit cell volume of 16.542
168 (23) $Å^3$, coexisting with an *fcc* lattice with a=3.211 (1) Å and a unit cell volume of
169 33.097 (30) $Å^3$. We find, within error, a similar atomic volume, V_A = 8.274 (7) $Å^3$ for
170 the *fcc* structure and V_A = 8.269 (11) $Å^3$ for the *hcp* structure and a large coexistence
171 domain which can be explained by the small enthalpy difference between the two
172 phases (6, 7, 13). These observations are in perfect agreement with the transition
173 pressure of 215-222 GPa reported in the previous X-ray diffraction work cited above
174 (13) or in the dynamic compression experiment (16). Alternatively, a slightly lower
175 pressure of 210 GPa is obtained when using another room temperature high-pressure
176 equation of state for aluminium (19). This *fcc* to *hcp* transition takes place at a
177 compression of 0.5, in general agreement with theoretical predictions (*e.g.* ref 7) or
178 experimental measurements (13).

179 In the second run, we explored pressures above 300 GPa. Patterns are cut at a maximum
180 angle of 20 degrees 2-theta because of the use of higher diamonds. With such a
181 configuration, diamond seats and cell mechanical opening prevented us to collect
182 diffraction at higher angles. In this second run (see Fig. 5), we also observe without
183 ambiguity the progressive growth of the *hcp* phase at the expense of the *fcc* phase, with
184 the complete disappearance of the *fcc* peaks at a pressure which can be estimated of
185 about 280 GPa according to the equation of state of aluminium (19) or that of rhenium
186 (18). In this run, the presence of rhenium reflections could not be avoided with a sample
187 chamber typically smaller than 8 μm as soon as pressure has been increased. At 235
188 GPa, lattice parameters a= 2.266 (1) Å and c=3.720 (2) Å for the *hcp* structure yield a
189 *c/a* ratio of 1.642 (2). At 370 GPa, with a= 2.182 (2) Å and c=3.557 (5), c/a ratio is

1.630 (4). It thus seems that the trend followed by *c/a* ratio is a decrease when pressure is increased. Between 320 GPa and 350 GPa, the most interesting feature is the observation of a splitting of the 002 reflection of the *hcp* structure (see Fig. 6). The remaining peaks corresponding to the *hcp* structure (100 and 101) do not show any significant broadening nor splitting. It is indeed shown in Fig. 6B and 6C that a new line here interpreted as the 110 *bcc* grows as a shoulder of the *hcp* 002 line. Some diffracted intensity detected around a 2–theta value of 17° close to the aluminium 102 *hcp* reflection (see Fig. 5) can tentatively be interpreted as the 200 *bcc* reflection.

Discussion

The *hcp* <-> *bcc* transformations with pressure are martensitic transitions which result from small relative movements of atoms. The *hcp* -> *bcc* transition has been studied in some detail from the theoretical point of view for the case of Mg (24, 25). It is thought to involve a distortion of the regular hexagonal atomic arrangement in the (001) *hcp* plane as well as a shear between adjacent (001) planes (see Figure 7). The distortion accounts for the transformation of the (001) *hcp* planes into the (110) *bcc* planes while the shear transforms the ABAB stacking along the [001] *hcp* direction to one compatible with the *bcc* structure. This mechanism principally involves the (001) *hcp* planes and would thus manifest itself by changes in peaks with 00l *hcp* character. This is exactly what we observe in our experiments as shown in Fig. 6 with a clear splitting of the 002 *hcp* line when pressure exceeds 320 GPa. It is expected the 002 *hcp* reflection should totally disappear with the appearance of a single 110 *bcc* peak when the transition is completed. However, it is likely the martensitic nature of such a transition makes the phase transition sluggish at ambient temperature where the

transformation is kinetically inhibited, as observed in other system at room temperature (see 26). Both low-pressure and high-pressure structures coexist on a large pressure domain and *hcp* reflections can still be observed at the pressure of 370 GPa as shown shown in Fig. 5 and 6, although the *bcc* features are less marked at this maximum pressure because of a diminution of the quality of our diffraction images. Though, our observations are compatible with the observations reported in the ramp-compressed aluminium experiment (16) where coexistence of the two high-pressure structures is no longer observed above 380 GPa. It is however likely kinetic barriers can be more easily overcome in shock experiments whereas it was impossible to heat up our sample kept under such pressure conditions in our experiment. We propose therefore that the peak splitting observed above 320 GPa correspond to the onset of the *hcp* to *bcc* structure transition, with compression along the [001] axis. In a rigid atom model, the *bcc->hcp* transition can be explained simply by using the relationships between atomic radius r and lattice parameters a_0 and c_0 with $a_0=2r$, $c_0\approx1.633a_0$ for *a hcp* structure and $a_0 = 4r/\sqrt{3}$ for a *bcc* structure, since the atomic packing fraction is higher in the *hcp* phase. In addition, the relations $a_{hcp}=\sqrt{3}a_{bcc}/2$ and $c_{hcp}=\sqrt{2}a_{bcc}$ can also be written for such a transition (see 27 for instance) and the cell parameters we could deduce from our experiments satisfy these relations. In our experiment, the unit cell volume fitted for the *hcp* structure at 320 GPa is V_{hcp}=15.655 (41) $Å^3$ while that calculated assuming that the split peak corresponds to 002 *bcc* yields V_{bcc}=15.719 (56), which are indiscernible within error bars at the onset of the transition. Observed pattern and reflections are shown for the two phases at 320 GPa in Fig.7. At this pressure, aluminium d-spacing for *bcc* 110 reflection is 1.771, which is comparable to values reported at the same pressure in (16).

We note that the transition to the *bcc* phase is predicted in the region between 290 and

310 GPa (6) or around 380 GPa (28) by first principles calculations, which respectively account for zero-point thermal vibrations or neglect these. These pressures compare well with the onset of the transition that we place at 320 GPa. We also have a perfect agreement with the 321 ± 12 GPa measured by velocimetry in the dynamic compression experiments (16). According to theoretical studies, the calculated enthalpy difference between these phases is only a few mRy (6, 7, 11) and one would experimentally expect these phases to co-exist over a large pressure range as in the case of the *fcc* to *hcp* transition. We can thus anticipate a very sluggish *hcp* to *bcc* transition. Our observations correspond to the first step of this transition, built here on a distortion of the *hcp* lattice.

Our experiment thus confirms the measured and predicted *fcc-hcp-bcc* phase transitions for Al. It also supports the predicted mechanism for this martensitic transition via a distortion and shear of the (001) *hcp* planes. Experiments permitting higher pressures than those reached here will be needed to detect a pure *bcc* phase unequivocally. Though a recent static pressure experiment has reached a pressure exceeding 1 TPa (29), our experiment performed on a sample of physical interest in conventional static pressure geometry, still opens new perspectives. It provides a large pressure window (up to 4 Mbar) for the study of a wide variety of materials and phenomena in conventional diamond-anvil cell geometry. These range from structural phase transitions or the detection of novel physical properties (such as superconductivity) in elemental or more complicated materials of physical or geophysical interest (30, 31).

Acknowledgements

The focused ion beam (FIB) and scanning electron microscopy (SEM) facility of the Institut de Minéralogie, de Physique des Matériaux et de Cosmochimie is supported by

Région Ile de France grant SESAME 2006 N°I-07-593/R, INSU-CNRS, INP-CNRS, University Pierre et Marie Curie-Paris 6, and by the French National Research Agency (ANR) grant ANR-07-BLAN-0124-01. G. Fiquet acknowledges the program MATISSE that contributed to the visit of Pr. Narayana at IMPMC-Sorbonne Université. MATISSE is a Cluster of Excellence led by Sorbonne Universités and managed by ANR within the Investissements d'Avenir program under reference ANR-11-IDEX-0004-02.

References:

1. J. A. Moriarty and A.K. McMahan, Phys. Rev. Lett. **48**, 809 (1982).

2. P. K. Lam and M. L. Cohen, Phys. Rev. B **26**, 5986 (1983).

3. A.K. McMahan and J. A. Moriarty, Phys. Rev. B **27**, 3235 (1983).

4. J.C. Boettger and S.B. Trickey, Phys. Rev. B **29**, 6434 (1984).

5. J.C. Boettger and S.B. Trickey, *Phys. Rev. B* **53**, 3007 (1996).

6. G.V. Sin'ko and N. A. Smirnov, J. Phys: Condens. Matter **14**, 6989 (2002).

7. F. Jona and P. M. Marcus, J. Phys: Condens. Matter **18**, 10881 (2006).

8. C.J. Pickard and R.J. Needs, Nature Mater. **9**, 624 (2010).

9. H. L. Skriver, Phys. Rev. B **31**, 1909 (1985).

10. A. Monza, A. Meffre, F. Baudelet, J.-P. Rueff, M. d'Astuto, P. Munsch, S. Huotari, S. Lachaize, B. Chaudret and A. Shukla, Phys. Rev. Lett. **106**, 247201 (2011).

11. H. Olijnyk and W. B. Holzapfel, Phys. Rev. B **31**, 4682, (1985).

12. H. K. Mao, Y. Wu, J. F. Shu, J. Z. Hu, R. J. Hemley and D. E. Cox, Solid State Comm. **74**, 1027, (1990).

13. Y. Akahama, M. Nishimura, K. Kinoshita, and H. Kawamura, Phys. Rev. Lett. **96**, 045505 (2006).

14. W.J. Nellis, J.A.Moriarty, A.C. Mitchell, M. Ross, R.G. Dandrea, N.W. Ashcroft, N.C. Holmes, and G.R. Gathers, Phys. Rev. Lett. **60**, 1414 (1988).

15. A. Vailionis, E.G. Gamaly, V. Mizeikis, W. Yang, A.V. Rode, and S. Juodkazis, Nat. Commun. **2:445**, doi 10.1038/nc omms1449 (2011).

16. D. N. Polsin, D. E. Fratanduono, J. R. Rygg, A. Lazicki, R. F. Smith, J. H. Eggert, M. C. Gregor, B. H. Henderson, J. A. Delettrez, R. G. Kraus, P. M. Celliers, F. Coppari, D. C. Swift, C. A. McCoy, C. T. Seagle, J.-P. Davis, S. J. Burns, G.W. Collins, and T. R. Boehly, Phys. Rev. Lett. **119**, 175702 (2017).

17. J. Orloff, C. Narayana, and A.L. Ruoff, Rev. Sci. Instr. **71**, 216 (2000).

18. S. Anzellini, A. Dewaele, F. Occelli, P. Loubeyre and M. Mezouar, J. Appl. Phys. **115**, 043511, doi 10.1063/1.4863300 (2014).

19. A. Dewaele, P. Loubeyre and M. Mezouar, Phys. Rev. B **70**, 094112 (2004).

20. L. Dubrovinsky, , N. Dubrovinskaia, , V.B. Prakapenka, and A.M. Abakumov, Nat. Commun. **3:1163** doi: 10.1038/ncomms2160 (2012).

21. A. Hammersley, S. Stevenson, M. Hanfland, A. Fitch and D. Häusermann, High Press. Res. **14**, 235 (1996).

22. A.C. Larson and R.B. Von Dreele, Los Alamos National Laboratory Report LAUR **86**–748 (2000).

23. B.H. Toby, J. Appl. Cryst. **34**, 210 (2001).

24. R. M. Wentzcovich and M. L. Cohen, Phys. Rev. B, **37**, 5571, (1988)

25. R. M. Wentzcovich, Phys. Rev. B, **50**, 10358, (1994)

26. H. Cynn, C.S. Yoo, B. Baer, V. Iota-Herbei, A.K. McMahan, M. Nicol and S. Carlson, Phys. Rev. Lett. **86**, 4552, 2001

27. Y. Yao and D.D. Klug, J. Phys. Condens. Matter **24**, 265401 (2012)

28. M.J. Tambe , N. Bonini, and N. Marzari, Phys. Rev. B **77**, 172102 (2008).

29. N. Dubrovinskaia, L. Dubrovinsky, N. A. Solopova, A. Abakumov, S.Turner, M. Hanfland, E. Bykova, M. Bykov, C. Prescher, V. B. Prakapenka, S. Petitgirard, I. Chuvashova, B. Gasharova, Y-L. Mathis, P. Ershov, I. Snigireva, A. Snigirev, Sci. Adv. **2**, e1600341 (2016).

30. C. Narayana, H. Luo, J. Orloff and A.L. Ruoff, Nature **393**, 46 (1998).

31. C-S. Zha, Z. Liu, and R.J. Hemley, Phys. Rev. Lett. **108**, 146402 (2012)

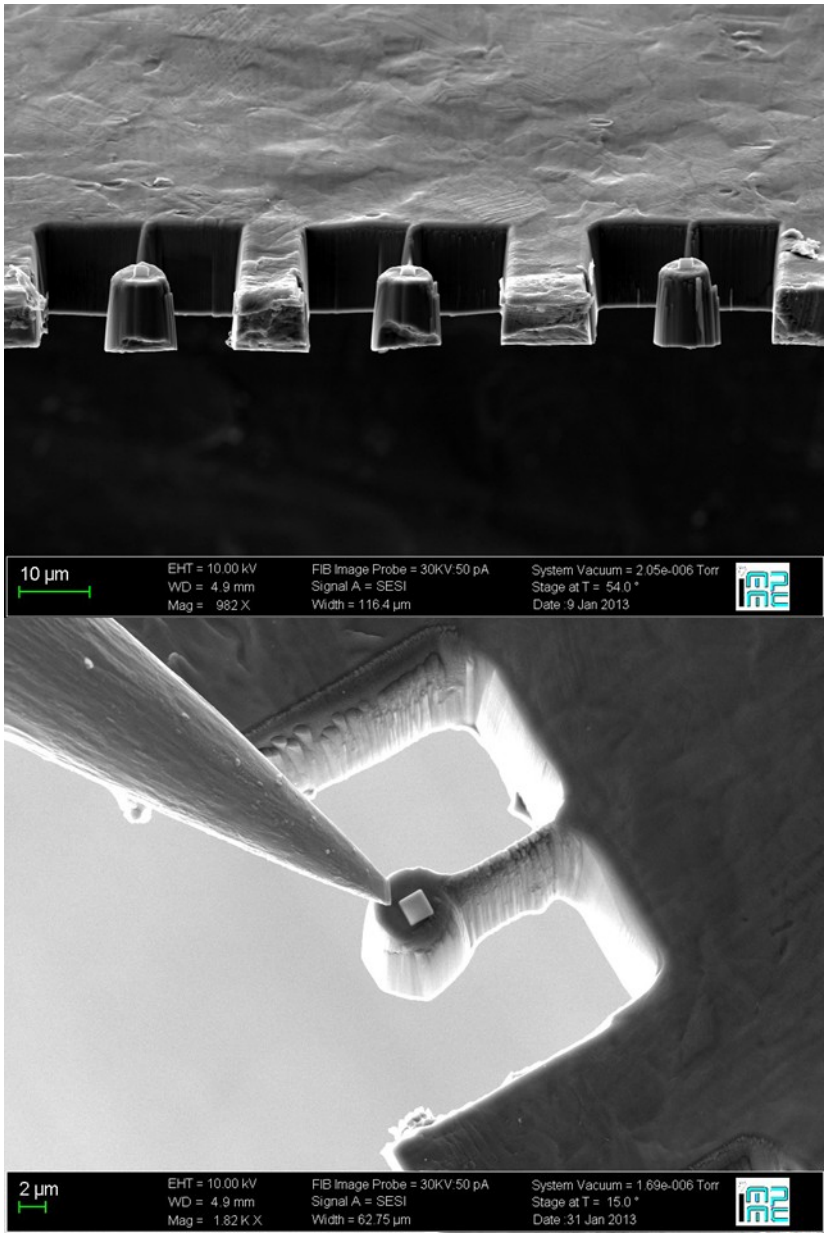

Figure 1. Secondary electron SEM images: series of sample cylinders shaped with focused ion beam (FIB) on the edge of the pure aluminium sample foil (top). Individual bulk aluminium sample piece during lift-out procedure. The small bridge holding the sample can easily be cut once micro-manipulator is attached. A platinum deposition (2 x 2 µm light square shape on the top) is visible (bottom). This pressure marker was unfortunately not detected during X-ray diffraction experiments.

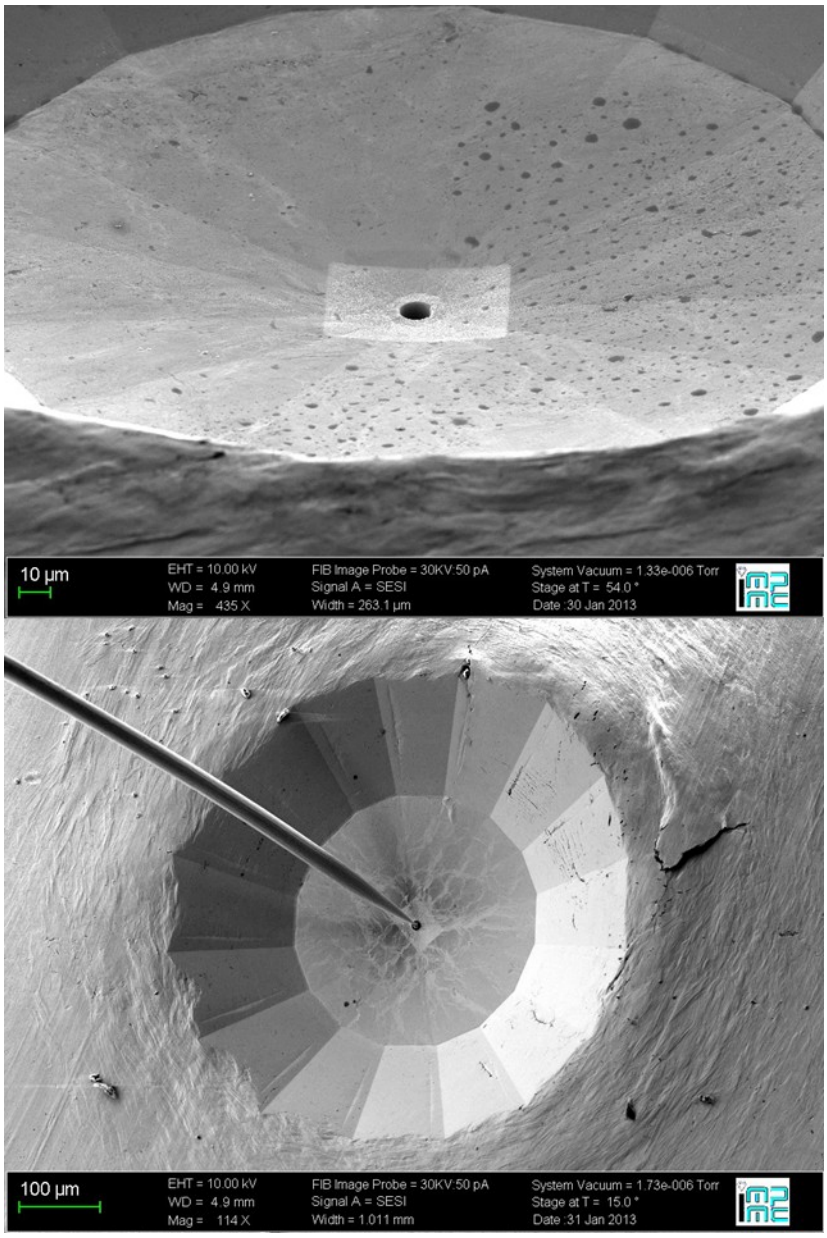

Figure 2. Secondary electron SEM images: 10 µm hole drilled with FIB at the center of the 20 µm inner culet print on the rhenium gasket. Outer culet is 300 µm in diameter (top). Sample cylinder loaded with micro-manipulator in sample chamber (bottom).

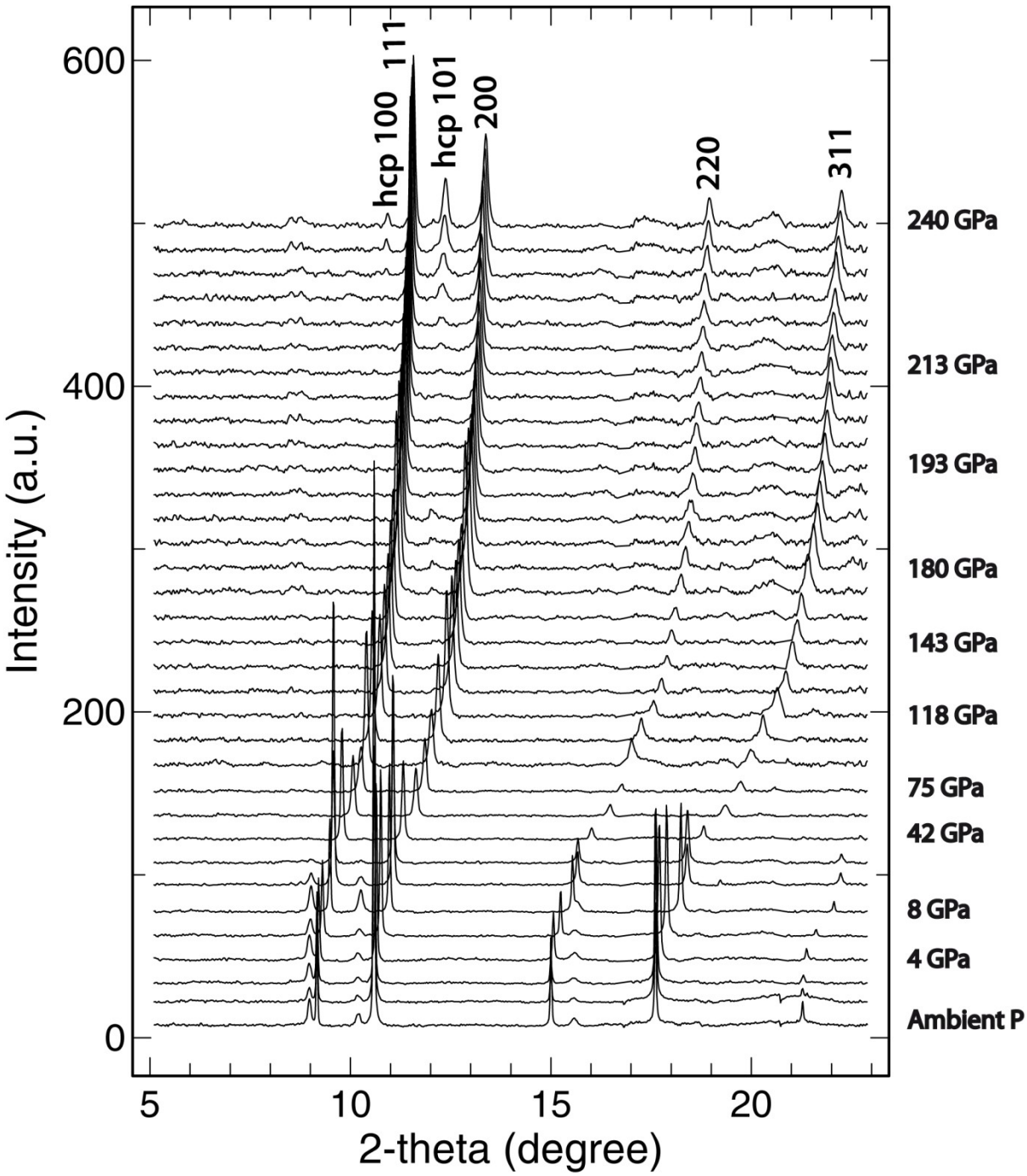

Figure 3. Diffraction pattern of an *fcc* aluminium sample compressed in a rhenium gasket at room temperature to 256 GPa in a diamond-anvil cell. Reflections corresponding to the hcp structure are detected at 213 GPa and pressures above.

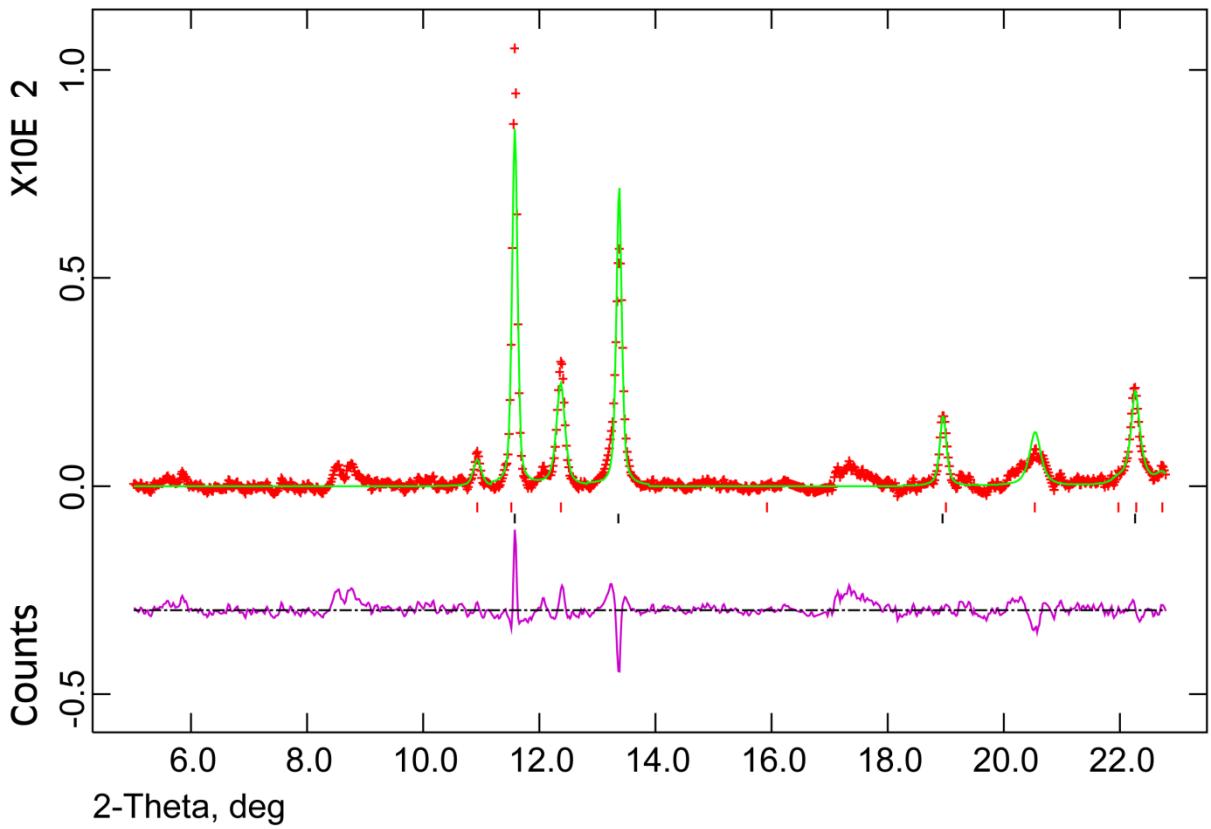

Figure 4. Analysis of X-ray diffraction pattern of aluminium collected at a pressure of 235 GPa, showing coexisting *fcc* and *hcp* structures. Cell parameters are a= 3.211 (1) Å and volume is V=33.097 (30) $Å^3$ for the *fcc* phase. Cell parameters are a=2.266 (1) Å and c=3.720 (2) Å with volume V=16.539 (23) $Å^3$ for the *hc*p phase.

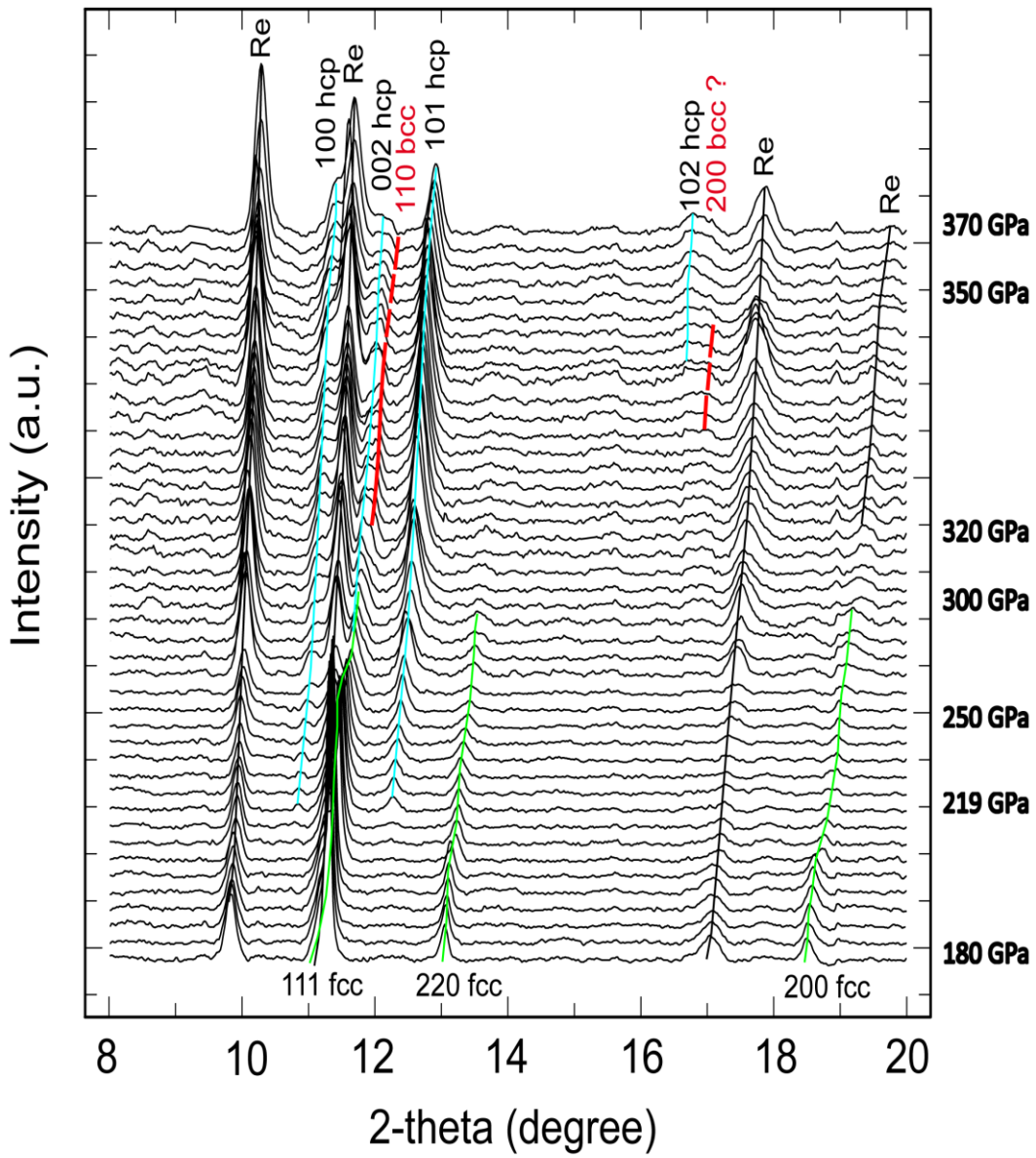

Figure 5. Series of full diffraction pattern collected between 180 to 370 GPa from bottom to top of the figure. Green lines (*fcc*), blue lines (*hcp*) and red lines (*bcc)* are guide to the eye for the different aluminium phases. The *fcc* phase is no longer observed at pressures exceeding 280 GPa. With the reduced size of the rhenium gasket pressure chamber, rhenium diffraction lines cannot be avoided at these pressures.

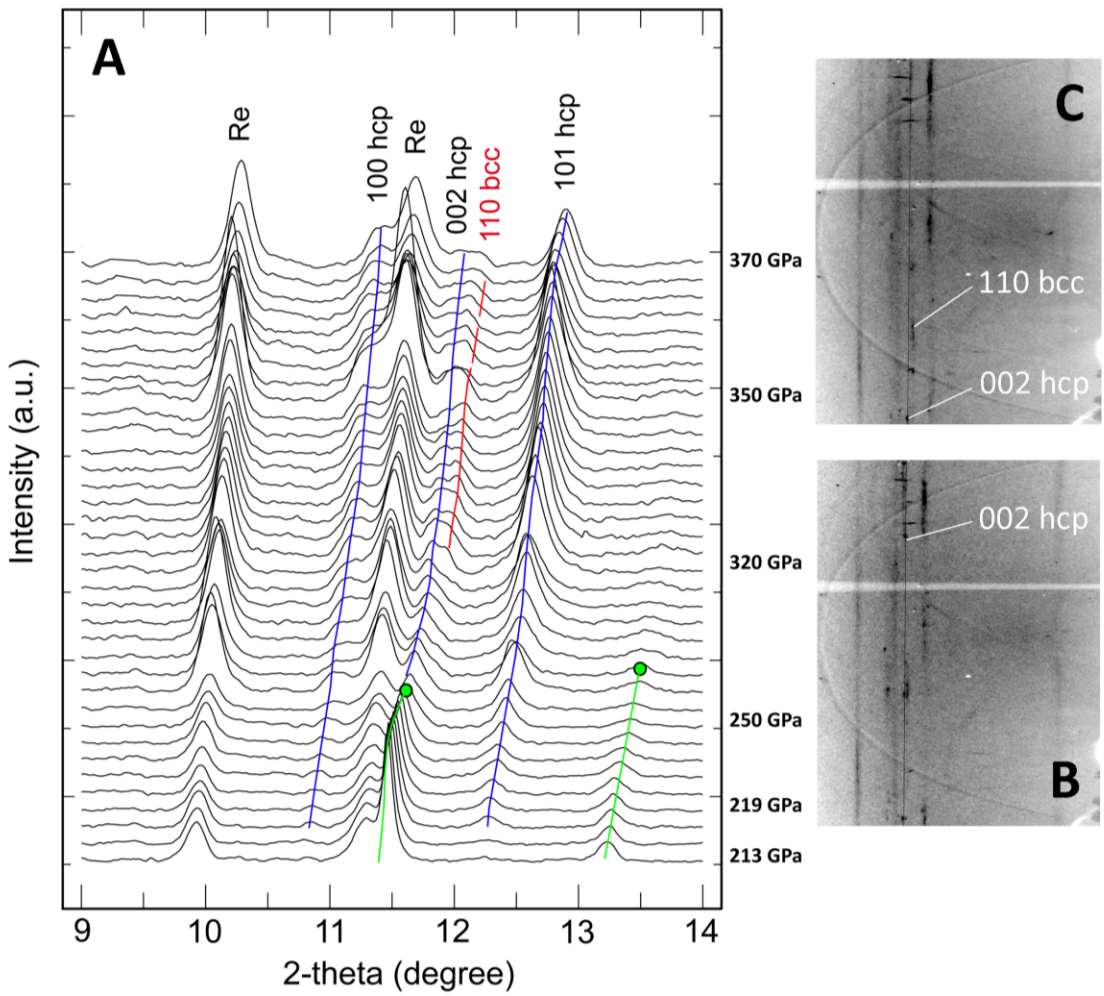

Figure 6. (A) Detailed view of the peak splitting observed at pressures above 320 GPa. Pattern collected between 280 to 370 GPa from bottom to top of the figure. Blue lines (*hcp*) and red lines (*bcc*) are guide to the eye for the different aluminium phases. (B) Cake image of the pattern recorded at 310 GPa, showing *hcp* 002 spotty reflections (C) Cake image of the pattern recorded at 330 GPa, showing the splitting of *hcp* 002 and *bcc* 110 reflections. A thin black line serves as a reference guide for the 002 *hcp* reflection.

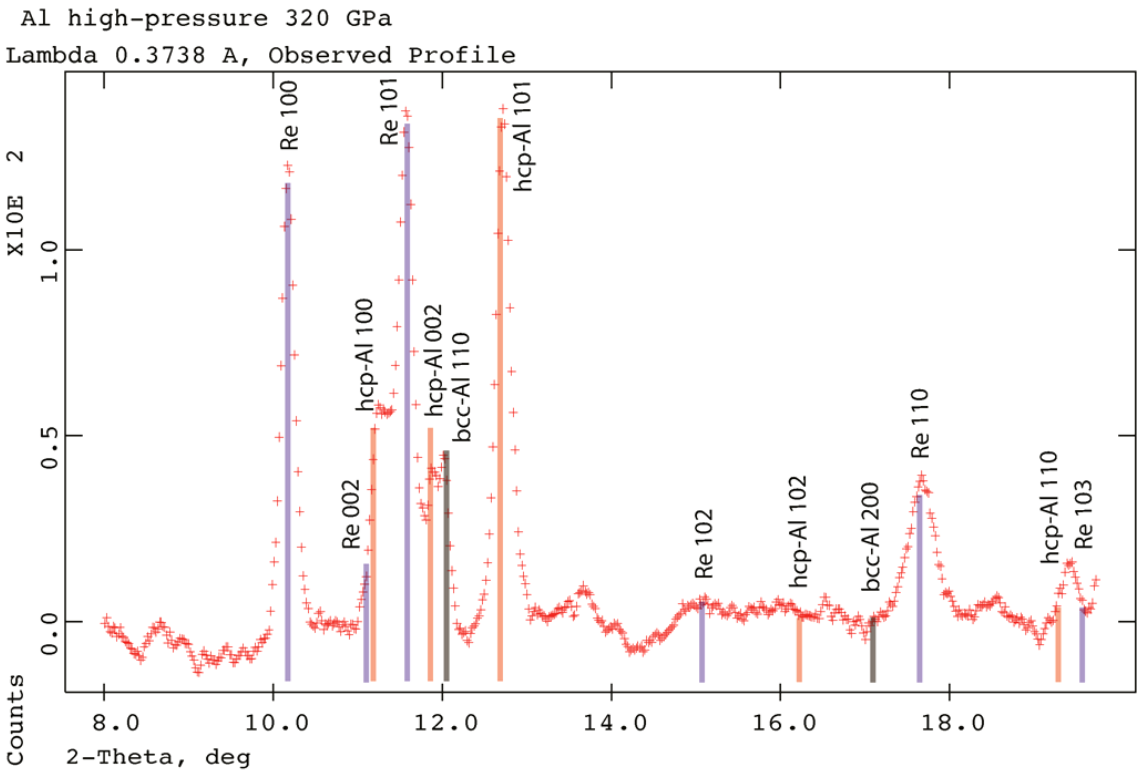

Figure 7. Observed diffraction at 320 GPa at the onset of the *hcp* – *bcc* transition. Fitted cell parameters are a= 2.230 (2) Å and c=3.635 (3) Å for a unit cell volume of 15.655 (41) $Å^3$ for the *hcp* structure, coexisting with a *bcc* lattice with a=2.505 (3) Å and a unit cell volume of 15.719 (56) $Å^3$.

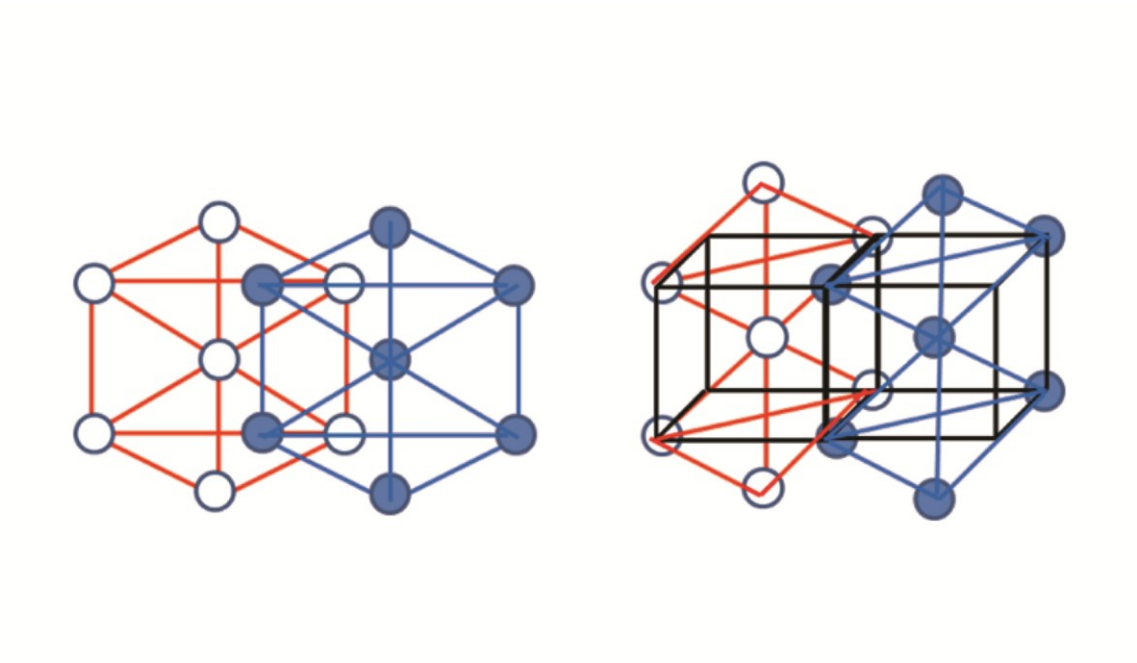

Figure 8. Left panel: View of adjacent (001) planes with ABAB stacking in the *hcp* structure, seen along the [001] axis. Right panel: View of adjacent (110) planes in the *bcc* structure derived from the (001) *hcp* planes by distortion and shear, with underlying *bcc* unit cells.